CANCER

A PSMA-targeted bispecific antibody for prostate cancer driven by a small-molecule targeting ligand

Sung Chang Lee[1†], Jennifer S. Y. Ma[1], Min Soo Kim[1‡], Eduardo Laborda[1], Sei-Hyun Choi[2§], Eric N. Hampton[1], Hwayoung Yun[2‖], Vanessa Nunez[1], Michelle T. Muldong[3], Christina N. Wu[4], Wenxue Ma[4], Anna A. Kulidjian[5], Christopher J. Kane[4], Vadim Klyushnichenko[1], Ashley K. Woods[1], Sean B. Joseph[1], Mike Petrassi[1], John Wisler[1], Jing Li[1], Christina A. M. Jamieson[3], Peter G. Schultz[1,2]*, Chan Hyuk Kim[1¶]*, Travis S. Young[1,2]*

Copyright © 2021 The Authors, some rights reserved; exclusive licensee American Association for the Advancement of Science. No claim to original U.S. Government Works. Distributed under a Creative Commons Attribution NonCommercial License 4.0 (CC BY-NC).

Despite the development of next-generation antiandrogens, metastatic castration-resistant prostate cancer (mCRPC) remains incurable. Here, we describe a unique semisynthetic bispecific antibody that uses site-specific unnatural amino acid conjugation to combine the potency of a T cell–recruiting anti-CD3 antibody with the specificity of an imaging ligand (DUPA) for prostate-specific membrane antigen. This format enabled optimization of structure and function to produce a candidate (CCW702) with specific, potent in vitro cytotoxicity and improved stability compared with a bispecific single-chain variable fragment format. In vivo, CCW702 eliminated C4-2 xenografts with as few as three weekly subcutaneous doses and prevented growth of PCSD1 patient-derived xenograft tumors in mice. In cynomolgus monkeys, CCW702 was well tolerated up to 34.1 mg/kg per dose, with near-complete subcutaneous bioavailability and a PK profile supporting testing of a weekly dosing regimen in patients. CCW702 is being evaluated in a first in-human clinical trial for men with mCRPC who had progressed on prior therapies (NCT04077021).

INTRODUCTION

Prostate cancer is the second most common cancer in men, which will affect one in nine men in the United States over the course of their lifetime (*1*). Treatment of localized disease (Gleason <6, PSA <10 ng/ml) by radiation, radical prostatectomy, or active surveillance is successful at controlling early-stage disease; however, relapse occurs in 20 to 50% of men (*2*). Patients who continue to progress on first- and second-line androgen deprivation therapies (ADT) develop castration-resistant prostate cancer (CRPC), which often metastasizes (mCRPC) to the bone, brain, liver, and lungs (*3*). Chemotherapies such as docetaxel and cabazitaxel have demonstrated improved survival in this population, but there is no cure for mCRPC (*4*).

Immunotherapies have demonstrated mixed success in prostate cancer. While the first cell-based immunotherapy sipuleucel T (Provenge) was approved in 2010 for mCRPC, checkpoint blockade targeting immunoinhibitory receptors PD-1 and CTLA-4 have shown markedly lower response rates in prostate cancer compared with other solid tumor malignancies (*5*). This is putatively due to the immunologically "cold" tumor microenvironment of primary prostate cancer tumors, characterized by low immune cell infiltration, and a weak neoantigen burden shown to be required for response to checkpoint blockade inhibitors (*6*). One way to circumvent this requirement for preexisting immunity to neoantigens is to directly recruit and activate effector T cells in a major histocompatibility complex–independent manner via engagement of CD3 on T cells with a bispecific antibody. Bispecific antibodies have been shown to increase T cell infiltration to tumors in preclinical models and to be active against quiescent stem cells and metastatic tumor cells, as well as those that have developed resistance to chemotherapy, making them a highly promising therapeutic modality (*7*–*9*). While this has been highly successful for treating hematological malignancies with the CD19-targeting bispecific blinatumomab, there is a high unmet need for further development in solid tumors. We and others have reported on the development of CD3 engaging bispecific antibodies targeting prostate-specific membrane antigen (PSMA, also known as glutamate carboxypeptidase 2 or folate hydrolase 1) for prostate cancer (*10*–*14*).

PSMA is an ideal prostate cancer target, predominantly expressed in the prostate epithelium with lower levels found on tissues outside the prostate (*15*). PSMA is highly up-regulated in all stages of prostate cancer, including bone metastases in mCRPC (*16*) after ADT (*17*, *18*), and is expressed on tumor-associated neovasculature (*19*). In addition to being a target for bispecific antibodies, PSMA has been targeted by multiple experimental therapies, including antibody-drug conjugates, chimeric antigen receptor–engineered T cells, and radiotherapeutics (*20*).

Here, we describe CCW702, a humanized, cynomolgus (cyno) cross-reactive, semisynthetic T cell–recruiting bispecific antibody targeting PSMA. CCW702 recruits T cells through a CD3-specific antibody Fab and selectively binds PSMA on prostate cancer cells via a synthetic small molecule inhibitor, 2-[3-(1,3-dicarboxy propyl)-ureido] pentanedioic acid (DUPA) (*10*, *21*, *22*). DUPA derivatives have been validated as imaging agents and radiotherapeutic ligands in more than a dozen clinically tested molecules (*23*). In our studies,

[1]Department of Biology, Calibr, The Scripps Research Institute, La Jolla, CA 92037, USA. [2]Department of Chemistry and Skaggs Institute for Chemical Biology, The Scripps Research Institute, La Jolla, CA 92037, USA. [3]Department of Urology, Moores Cancer Center, University of California, San Diego, La Jolla, CA 92093, USA. [4]Department of Medicine, Moores Cancer Center, University of California, San Diego, La Jolla, CA 92093, USA. [5]Department of Orthopedic Surgery, Scripps MD Anderson Cancer Center, La Jolla, CA 92093, USA.
*Corresponding author. Email: schultz@scripps.edu (P.G.S.); kimchanhyuk@kaist.ac.kr (C.H.K.); youngtr@scripps.edu (T.S.Y.)
†Present address: Therabest USA, San Diego, CA 92121, USA.
‡Present address: Department of Global Biologics, Takeda California Inc., San Diego, CA 92121, USA.
§Present address: Innovo Therapeutics Co. Ltd., Daedeok Biz Center, Techno Valley, Yuseong-gu, Daejeon 34013, Republic of Korea.
‖Present address: College of Pharmacy, Pusan National University, Busan 46241, Republic of Korea.
¶Present address: Department of Biological Sciences, Korea Advanced Institute of Science and Technology, Daejeon 34141, Republic of Korea.

we demonstrate that CCW702 binds to PSMA with high specificity and cross-links tumor cells to T cells, resulting in T cell activation and target cell lysis akin to the function of a bispecific antibody. Profiling of CCW702 demonstrates high potency in vitro and in vivo with good tolerability and subcutaneous bioavailability in nonhuman primate models. CCW702 is currently being evaluated in a phase 1 clinical trial in patients with mCRPC.

RESULTS

Optimization of a humanized, cyno cross-reactive DUPA-CD3 conjugate bispecific antibody

In our previous studies, we demonstrated that increased binding affinity to PSMA correlates with enhanced in vitro efficacy of PSMA-targeting bispecific antibody conjugates (Fig. 1A) (*10*). To increase the affinity of DUPA for PSMA, we used structure-based design to develop DUPA-linker analogs that target both the PSMA glutamate-urea–binding active site and two hydrophobic binding pockets distal and proximal to the active site (*24*, *25*). To optimize the hydrophobic interactions, the C9 amide in P-Phthal (p-phathalamide) [first-generation candidate (*10*)] was substituted with bioisostere 1,2,3-triazole that improved the polarization of the interaction. The linkage to the second aromatic group phthalimide was optimized to include a short hydrocarbon chain to create P-TriA (triazole) (Fig. 1B). In an enzymatic inhibition assay using recombinant PSMA, P-TriA demonstrated substantially enhanced (~400-fold) inhibitory activity compared with P-Phthal and a 1600-fold increase in inhibitory activity [inhibition constant (K_i) = 0.005 nM] compared to DUPA alone (fig. S1), indicating that enhanced P-TriA bidentate binding is a result of the two identified hydrophobic pockets.

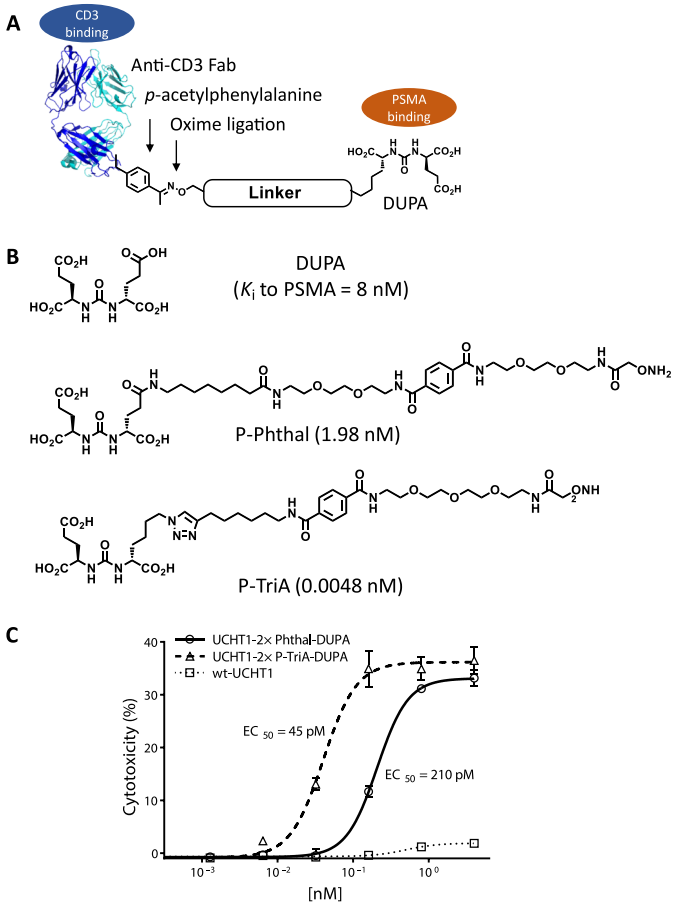

Fig. 1. Affinity optimization of DUPA. (**A**) General structure of the DUPA–linker–anti-CD3 Fab (DUPA-CD3) conjugate showing the unnatural amino acid *p*-acetylphenylalanine and oxime ligation (bond) formed between the ketone and amino-oxy group. (**B**) Chemical structures of DUPA and DUPA with P-Phthal, and P-TriA linkers with measured PSMA inhibition constant (K_i) shown from fig. S1. (**C**). In vitro cytotoxicity assay by lactate dehydrogenase (LDH) release, of coculture of PBMCs with C4-2 cells [E:T (Effector to Target ratio) = 10:1], 24 hours, comparing dose titration of UCHT1-2× Phthal-DUPA and UCHT1-2× P-TriA-DUPA with wild-type (wt) UCHT1 Fab that was not conjugated to DUPA. UCHT1 is the anti-CD3 antibody clone used in (*10*). Each data point is a mean of three samples, and error bars represent SD. Sigmoidal dose response (variable slope) curve fit was applied.

To compare the in vitro activity of P-Phthal to P-TriA, the molecules were conjugated to two *p*-acetylphenylalanine residues incorporated via unnatural amino acid mutagenesis in the heavy and light chains (HC and LC, respectively) of the Fab region from the previously reported anti-CD3 antibody clone UCHT1 (fig. S2) (*10*). Briefly, conjugation was carried out by incubation of the DUPA-linker under pH 4.5 to form the oxime bond between the amino-oxy group of the linker and the ketone of the pAcF (*p*-acetylphenylalanine) residue. This reaction enabled nearly 100% site-specific DUPA conjugation efficiency at a 2:1 stoichiometry as previously reported (*10*). Comparison of the in vitro activity against prostate cancer cells in a coculture assay with human peripheral blood mononuclear cells (PBMCs) and PSMA-positive C4-2 tumor cells demonstrated that the UCHT1-P-TriA-DUPA conjugate exhibited fivefold greater potency [median effective concentration (EC_{50}) = 45 pM)] compared with UCHT-Phthal-DUPA conjugate (EC_{50} = 210 pM) (Fig. 1C).

The UCHT1 anti-CD3 antibody does not cross-react with nonhuman primate, which precludes toxicology assessment in a relevant higher species, such as the cynomolgus monkey. To develop such a candidate, we humanized a cynomolgus-monkey cross-reactive antibody clone (murine origin) using CDR (complementary determining region) grafting to human germline frameworks with accompanying stability mutations to create clone huL5H2. Binding of huL5H2 to cynomolgus monkey $CD3^+$ HSC-F cells was within twofold of binding to human $CD3^+$ Jurkat cells by flow cytometry (EC_{50} = 3.76 nM versus 5.92 nM, respectively) (Fig. 2, A and B).

To determine the likelihood of huL5H2 to produce an antidrug antibody (ADA) response in patients, we used in silico analysis for potential T cell epitopes. This assessment identified a low potential for immunogenicity in LC L5 (score, −38.57) but a high potential for immunogenic response to HC H5 in human (score, 27.74) by regulatory T cell (T_{reg})–adjusted EpiMatrix score (fig. S3). To address this, we identified four HC mutations (K19R, S41P, K89R, and T90A) to remove these liabilities. These mutations further introduced potential Tregitopes, which significantly reduced the T_{reg}-adjusted immunogenicity score to −51.19 (*26*, *27*). These mutations alone, or in combination (referred to hereafter as huL5H2_DI), had minimal impact on the binding affinity to both human and cynomolgus T cells (Fig. 2, A and B). Thus, clone huL5H2_DI was used for further development.

Next, we sought to optimize valency for the huL5H2_DI clone. Leveraging the site-specific nature of the pAcF-mediated conjugation, we tested conjugation of P-TriA to the HC (1× HC at residue K141), the LC (1× LC at residue S205), or both chains (2× LC/HC) of the huL5H2_DI Fab. In vitro coculture assays with human PBMCs

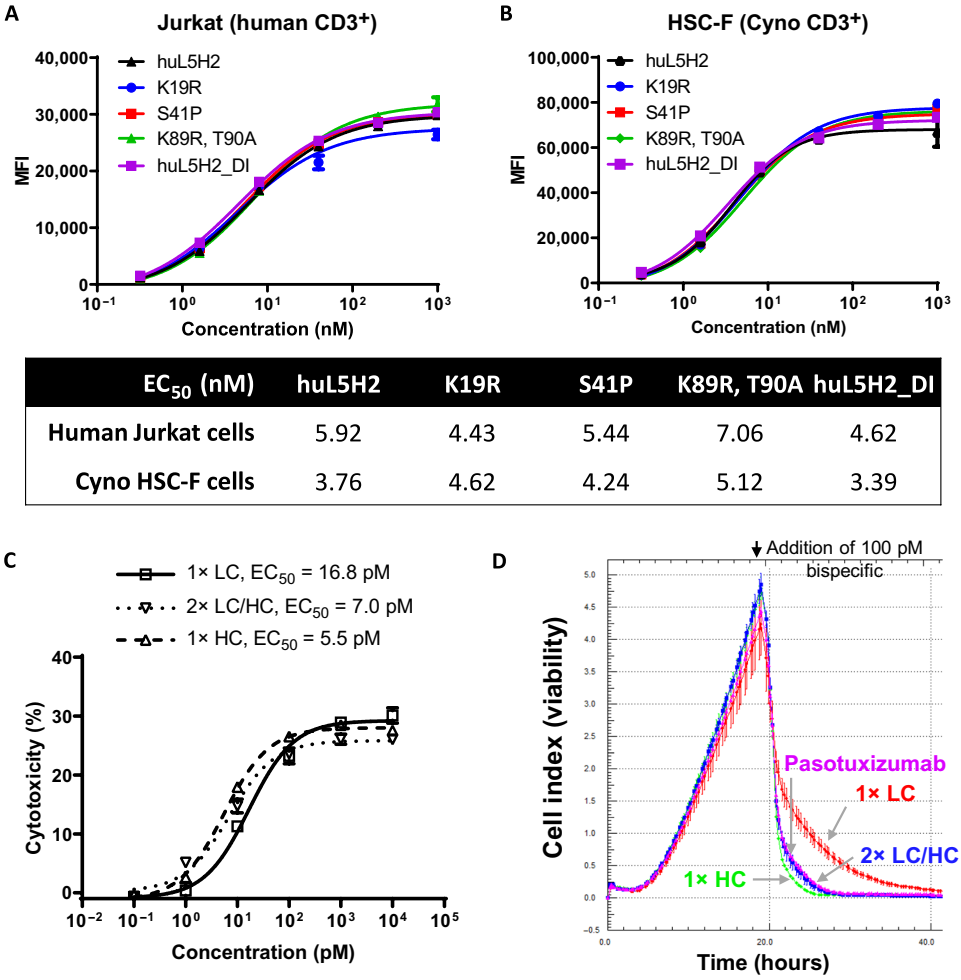

EC_{50} (nM)	huL5H2	K19R	S41P	K89R, T90A	huL5H2_DI
Human Jurkat cells	5.92	4.43	5.44	7.06	4.62
Cyno HSC-F cells	3.76	4.62	4.24	5.12	3.39

Fig. 2. Characterization of deimmunized and optimized Fab-DUPA conjugates. Flow cytometry–based binding curves of deimmunized anti-CD3 Fab (huL5H2_DI)–2× P-TriA-DUPA conjugates to (**A**) human $CD3^+$ Jurkat cells and (**B**) cynomolgus monkey $CD3^+$ HSC-F cells. MFI, mean fluorescence intensity. EC_{50} (nM) by sigmoidal four parameter logistic (4PL) curve fit is tabulated below. (**C**) In vitro cytotoxicity assay by LDH release of coculture of PBMCs with C4-2 cells (E:T = 10:1), 24 hours, of candidate huL5H2_DI–P-TriA-DUPA by monovalent 1× LC or 1× HC, or bivalent 2× LC/HC. (**D**) Real-time cytotoxicity assay (XCELLigence) comparing 1× HC (green), 1× LC (red), 2× LC/HC (blue), and pasotuxizumab comparator (purple), each at 100 pM. Full curves at range of concentrations shown in fig. S4.

and target C4-2 cells demonstrated that the potency of designs followed the trend 1× HC > 2× LC/HC > 1× LC (Fig. 2C). By monitoring the kinetics of cytotoxic activity induced by the bispecific antibodies, we further confirmed that the 1× LC design elicited the slowest rate of cytotoxicity from PBMCs compared with 1× HC, 2× LC/HC, or fully recombinant control BiTE, pasotuxizumab (Fig. 2D). Of these molecules tested, 1× HC exhibited the fastest rate of cytotoxicity.

To further profile the activity of 1× HC and 2× LC/HC, we cocultured PBMCs in vitro with PSMA-positive C4-2 cells or PSMA-negative DU145 cells and assayed them for target cells lysis, T cell cytokine production, up-regulation of CD25 and CD69 activation markers on T cells, and induction of T cell proliferation (Fig. 3, A to D). Corresponding with the mechanism of action, both 1× HC and 2× LC/HC induced dose-dependent T cell proliferation in the presence of C4-2 cells (Fig. 3D). Neither 1× HC nor 2× LC/HC lysed or elicited cytokine production or up-regulation of activation markers on human T cells in the presence of DU145 cells, indicating that binding of CCW702 to T cells does not cause activation in the absence of cross-linking to target (PSMA). Overall, 1× HC induced more potent cytotoxicity, induced greater cytokine production, and up-regulated activation markers on T cells significantly better than the 2× LC/HC design. Thus, the 1× HC construct was chosen for further development under the name CCW702.

In vitro characterization of CCW702

Profiling of CCW702 demonstrated that the semisynthetic format was stable and well behaved. CCW702 exhibited a thermal melt temperature (T_m) of 72°C by differential scanning fluorimetry and little to no high–molecular weight (HMW) species after storage in phosphate-buffered saline (PBS) at 4°C for 2 weeks (fig. S5). This was compared with the bispecific single-chain variable fragment (bis-scFv) comparator (pasotuxizumab), which had a T_m = 65°C and 3.5 to 4% HMW species under the same conditions, consistent with reports for bis-scFv formats (*28*). CCW702 was also stable in serum and exhibited no loss or gain of potency or change in molecular weight by high-resolution mass spectrometry in mouse, human, and nonhuman primate serum for 48 hours (fig. S6). Thus, the oxime linkage between the P-TriA-DUPA and the ketone of the

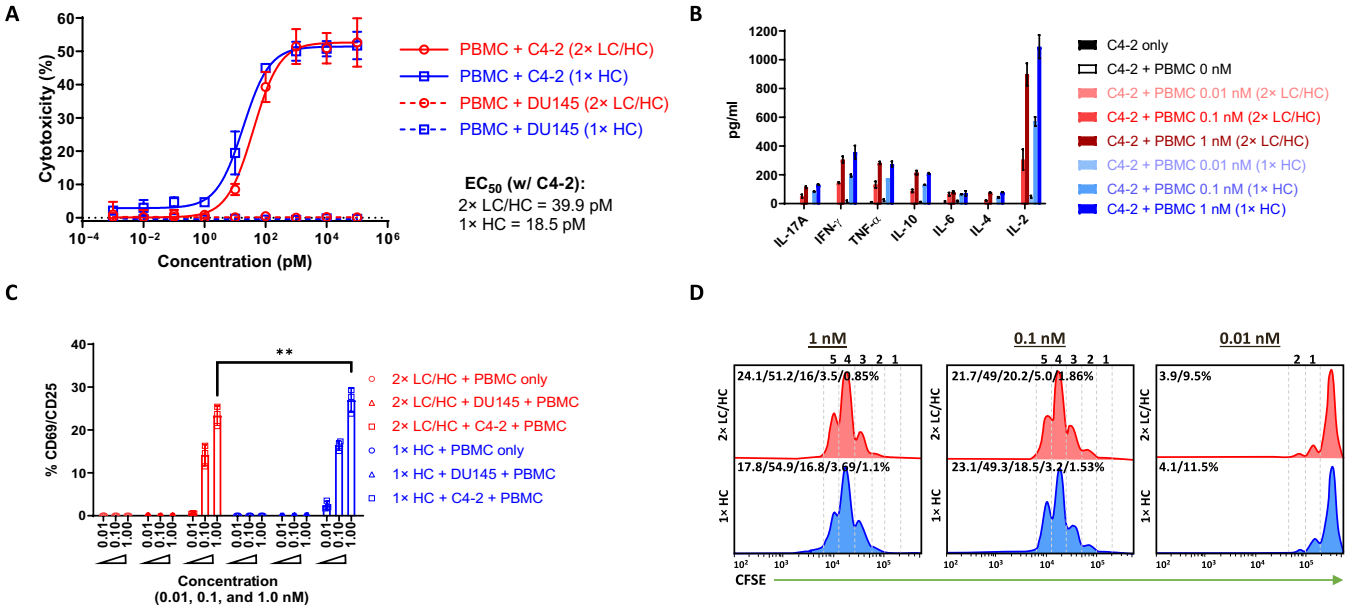

Fig. 3. Functional comparison of bivalent (2× LC/HC) versus monovalent (1× HC) DUPA-CD3 conjugates. (**A**) In vitro cytotoxicity by LDH release of coculture of PBMCs with PSMA-positive C4-2 or PSMA-negative DU145 prostate cancer cells (E:T = 10:1), 24 hours. (**B**) Cytokine release from PBMCs in culture conditions from (A). Supernatants from cocultures were taken after 24 hours and shown for C4-2 for 0.01, 0.1, and 1.0 nM 2× LC/HC or 1× HC conjugates. Little to no cytokines were detectable from coculture with DU145. (**C**) Up-regulation of T cell activation markers CD25 and CD69 (% double-positive cells) by flow cytometry following coculture conditions in (A). $^{**}P \leq 0.0021$ significance by two-way analysis of variance (ANOVA). (**D**) T cell proliferation after coculture with C4-2 cells and DUPA–anti-CD3 conjugates by carboxyfluorescein succinimidyl ester (CFSE) dilution in flow cytometry after 72 hours (E:T = 1:1). Population doublings are shown above graphs with percentage cells in each doubling listed in inset. In (A) to (D), 2× LC/HC candidates are shown in red and 1× HC in blue.

pAcF unnatural amino acid residue of the anti-CD3 Fab had no overt metabolic liability.

CCW702 demonstrated comparable affinities for human, cynomolgus monkey, and mouse PSMA by biolayer interferometry (Octet) (Fig. 4A and fig. S7). CCW702 also bound comparably to human and cynomolgus monkey CD3 but not to mouse CD3, consistent with the species reactivity of the parent clone (*29*). The affinity of CCW702 was approximately sixfold stronger for human PSMA than for human CD3 (1.41 ± 0.67 nM versus 8.58 ± 1.91 nM, respectively).

To determine the most sensitive biological marker of activity, we profiled CCW702 with full-dose titration for cytotoxicity, cytokine production, and up-regulation of activation markers in the presence of PSMA-positive C4-2 target cells with two sets of healthy donor–derived PBMCs (Fig. 4B and fig. S8). Of these assessments, cytotoxicity was the most sensitive marker of in vitro biological activity compared with cytokine release and up-regulation of activation markers, consistent with reports for other T cell–engaging bispecific antibodies (*30*). Insignificant cytotoxicity, cytokine release, or activation of T cells was observed in the presence of PSMA-negative DU145 cells even at 100 nM CCW702, indicating a lack of antigen-independent T cell activation.

Next, the impact of soluble and of the cell-surface density of PSMA on CCW702 activity was evaluated. Toward this end, five cell lines, LNCaP, C4-2, VCaP, 22Rv-1 (sorted), and 22Rv-1 (parent), and PSMA-negative DU145 cells were enumerated for PSMA antigen density using quantitative flow cytometry (Fig. 4C and fig. S9). In vitro cytotoxicity by coculture assay with human T cells demonstrated a sigmoidal relationship between antigen density and the EC_{50} of in vitro potency. Soluble PSMA had insignificant impact on the activity of CCW702: No inhibition of activity was observed up to approximately 10,000 pM soluble PSMA (approximately 10^3-fold above the EC_{50} of CCW702) using a competition assay with Jurkat NFAT-luciferase cells cocultured with C4-2 cells (Fig. 4D). This concentration of PSMA is above what has been reported for detection of soluble PSMA in serum and thus is not expected to have a significant impact on activity (*31*, *32*).

In vivo efficacy in xenograft and patient-derived xenograft models

To determine exposure of CCW702 in non–severe combined immunodeficient γ (NSG) mice, we carried out pharmacokinetic studies as a single intravenous and subcutaneous dosing. Subcutaneous administration exhibited a half-life of 5.1 hours and 39% bioavailability (in PBS) (fig. S10); therefore, subcutaneous dosing was pursued in mouse models.

Efficacy was tested in the C4-2 xenograft model in NSG mice with immune function reconstituted with human T cells [2×10^7 cells, intraperitoneally (ip)]. Three subcutaneous treatment regimens were compared: Every other day (QAD) at three-dose levels (0.15, 0.7, and 3.5 mg/kg; groups D to F, respectively), every 7 days (Q7D) at four-dose levels (1.13, 3.5, 11.1, and 35.2 mg/kg; groups G to J), or every 4 days (Q4D) at one-dose level (3.5 mg/kg; group L). A PSMA-targeted bispecific antibody comparator, pasotuxizumab, was dosed at 3.75 mg/kg every day (QD) for 28 days as previously reported (*12*). On the basis of the reported clearance for pasotuxizumab in NSG mice, this dose was expected to afford exposure similar to that of the 0.7 mg/kg QAD group for CCW702.

Tumors were eliminated to below detection limits in the majority of mice (>50% at the end of the dosing period) in groups treated

A

Test	Ligand	Analyte	KD (nM)
Hu CD3	Hu CD3δ/ε-Fc	CCW702	8.58 ± 1.91
Cy CD3	Cy CD3δ/ε	CCW702	8.15 ± 1.06
Mu CD3	Mu CD3δ/ε-Fc	CCW702	n/a
Hu PSMA	Hu PSMA	CCW702	1.41 ± 0.67
Cy PSMA	Cy PSMA	CCW702	3.36 ± 0.06
Mu PSMA	Mu PSMA	CCW702	2.66 ± 0.45

B

(pM)	Cytox	CD69	CD25	TNFα	INFγ	IL-2
EC_{90}	60.6	208	299	168	444	161
EC_{50}	10.8	27.1	44.3	33.9	82.2	104
EC_{20}	3.6	7.5	13.3	12.4	28.8	87.3

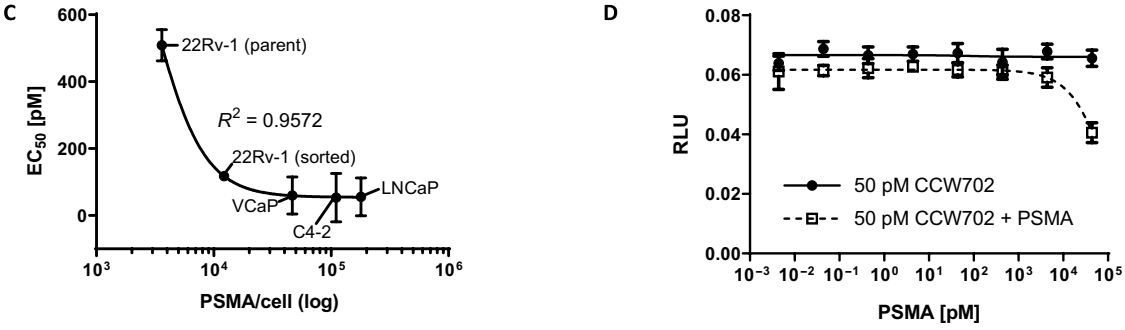

Fig. 4. Profiling of CCW702 in vitro binding and activity. (**A**) Octet binding affinities of CCW702 (huL5H2_DI-1× P-TriA-DUPA) to recombinant PSMA and CD3 (δ/ε chains) from mouse, cynomolgus monkey, and human. Hu, human; Cy, cynomolgus; Mu, murine; and K_D, dissociation constant. (**B**) Summary table of in vitro cytotoxicity, cytokine production, and up-regulation of activation markers CD69 and CD25 of PBMCs cocultured with a dose titration of CCW702 in the presence of PSMA-positive C4-2 target cells, average of two normal donor-derived PBMCs. Curve fits by sigmoidal 4PL are shown in fig. S8. (**C**) Correlation (sigmoidal, 4PL) between surface expression of PSMA in human prostate cancer cell lines (quantified by flow in fig. S9) and in vitro cytotoxicity [shown in (B)]. Parental 22Rv-1 cells exhibited two distinct population on PSMA expression; sorting of 22Rv-1 cells was performed to enrich for PSMA-expressing cells. (**D**) Effect of soluble PSMA on CCW702-mediated T cell activation via Jurkat-NFAT-luc cells, 20 hours at 37°C. RLU, relative light units. Each data point is a mean of three samples, and error bars represent SD.

with CCW702 QAD, Q4D, or doses >3.5 mg/kg Q7D, and in mice treated with the comparator pasotuxizumab (Fig. 5, A and B, and fig. S11). The 1.1 mg/kg Q7D group significantly reduced tumor burden but did not completely clear tumors by the end of the dosing period, indicating that the minimal efficacious dose in this model had been reached. Body weight loss was observed with CCW702 treatment but was generally transient and recovered through the course of the study (fig. S12).

Human cytokines interferon-γ (IFN-γ), interleukin-2 (IL-2), and tumor necrosis factor–α (TNF-α) measured in plasma at 24 hours after the first dose of CCW702 exhibited a dose-dependent increase for IFN-γ and TNF-α, while IL-2 remained relatively consistent over the dose range (fig. S13). Very low levels of cytokines were observed in the pasotuxizumab group, putatively because of the lack of cross-reactivity of pasotuxizumab with mouse PSMA compared with the high affinity of CCW702 to mouse PSMA. Human $CD3^+$, $CD4^+$, and $CD8^+$ T cells counts in peripheral blood on day 18 exhibited an inverse relationship to cytokines with decreasing counts at the highest doses of CCW702 (fig. S14). This was expected to be due to T cell extravasation upon T cell activation as previously reported and is a useful pharmacodynamic marker (*33*, *34*).

CRPC metastases commonly take residence in the bone. To evaluate the efficacy of CCW702 on primary, patient-derived tumors, we tested potency on Prostate Cancer San Diego 1 (PCSD1) primary, patient-derived cells. The PCSD1 model closely mimics the bone metastatic disease that manifests in the patient with prostate cancer, which includes mixed osteolytic and osteoblastic bone lesion formation and resistance to ADT, specifically in the bone (*35*–*37*). CCW702 exhibited cytotoxic potency against PCSD1 (EC_{50} = 10.0 pM, average two donors) that was comparable to C4-2 in in vitro coculture assays (fig. S15). This was consistent with PCSD1 and C4-2 expressing similar levels of PSMA (approximately 10^5 PSMA per cell).

In vivo treatment of PCSD1 tumors was tested using an intrafemoral inoculation of tumors in NSG male mice, with immune function reconstituted with human T cells (2×10^7 cells, ip). CCW702 was administered daily, intravenously, for 10 doses at 0.2 mg/kg. Although treatment with T cells alone had some impact on tumors, because of potential alloreactivity of donor T cells, tumors treated with T cells and CCW702 were eliminated to near the limit of detection by caliper measurement and demonstrated significant decrease in tumor luminescence at the end of the dosing period (Fig. 5C and fig. S16). Treatment with CCW702 only had no effect on tumor growth compared with vehicle control. Tumors in the CCW702 group showed resumed growth after the initial dosing, between days 50 and 60 of the model. Retreatment with CCW702 eliminated relapsed tumors to near the limit of detection.

Pharmacokinetics and pharmacodynamics in nonhuman primate

To guide CCW702 dose selection in humans, we carried out a series of pharmacokinetic studies in cynomolgus monkey using subcutaneous and intravenous routes of administration. CCW702 exposure was detectable by electrochemiluminescence bioanalytical assay at doses of ≥9.8 μg/kg. Noncompartmental analysis of subcutaneous and intravenous data demonstrated that apparent clearance was comparable, whereas volume of distribution was six times larger for the subcutaneous route compared to the intravenous route. Subcutaneous dosing had near complete bioavailability (F = 108 ± 20.2%) with a maximum concentration (C_{max}) and half-life ($t_{1/2}$) of 1.5 (ng/ml)/(mg/kg) and 11.4 hours compared with the intravenous

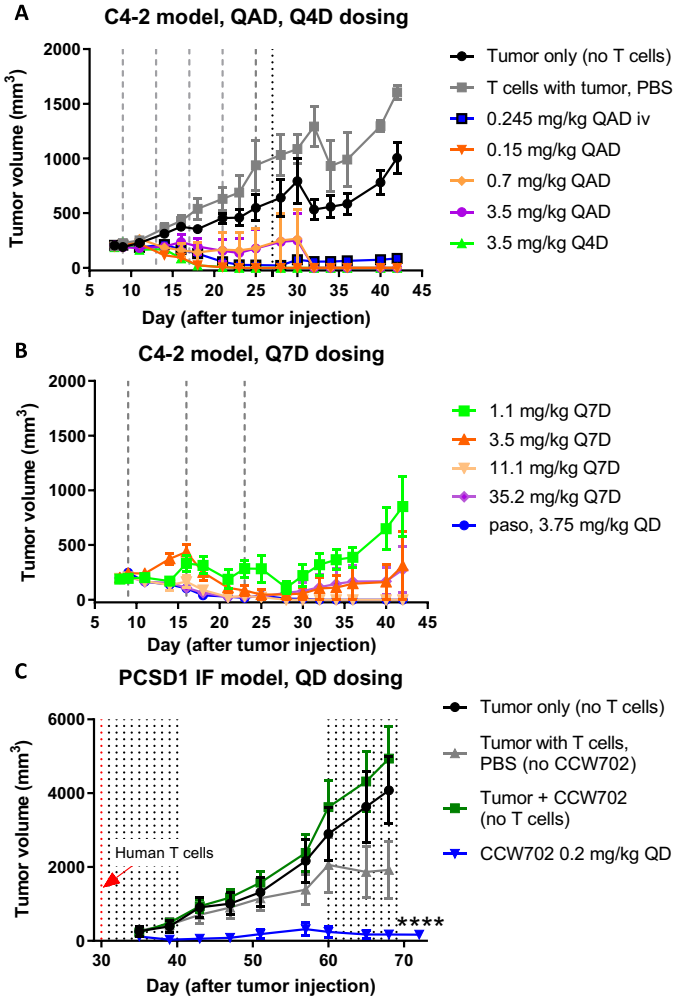

Fig. 5. CCW702 in vivo antitumor efficacy in xenograft models in immunodeficient NSG mice. (**A** and **B**) CCW702 dose titration in C4-2 xenograft with dosing of CCW702 and pasotuxizumab every other day (QAD) and every 4 days (Q4D) or every 7 days (Q7D). CCW702, pasotuxizumab, and controls were dosed subcutaneously except where indicated as intravenously (iv). CCW702 tumors were injected subcutaneously on day 0; 20×10^6 expanded human T cells were delivered intraperitoneally on day 7, followed by treatment initiation on day 8, $n = 7$ per group. Spider plots and body weight for each group and individual mouse are shown in figs. S11 and S12. (**C**) CCW702 antitumor efficacy in a bone metastasis patient-derived xenograft (PDX) model, PCSD1. CCW702 was administered intravenously, 0.2 mg/kg, daily for 10 days starting at days 31 and 60. PCSD1 tumors were injected intrafemorally on day 0; 20×10^6 expanded human T cells were delivered intraperitoneally at day 30, followed by treatment initiation at day 31, $n = 10$ per group. BLI (Bioluminescence imaging) is shown in fig. S16. For both models, data shown represent mean tumor volume ± SEM. Dotted lines indicate administration of described treatment. Significance, ****$P \leq 0.0001$ by two-way ANOVA and Tukey's multiple comparisons post-test. IF, intrafemoral.

route of administration C_{max} of 28.3 (ng/ml)/(mg/kg) and $t_{1/2}$ of 1.6 hours, respectively (fig. S17). The large volume of distribution estimated from the subcutaneous data is consistent with a slow absorption rate constant. The elimination following subcutaneous administration appears to be limited by lymphatic absorption rate. While the systemic elimination rate was around 2 hours, lymphatic absorption and subsequent delivery of CCW702 to the systemic circulation occurred much more slowly, effectively increasing the duration of the molecule in systemic circulation, a hallmark of flip-flop kinetics (*38*).

A repeat dose administration study was carried out to determine tolerability and pharmacodynamic effects of CCW702 on peripheral blood T cell redistribution and serum cytokine levels in cynomolgus monkey. Doses of 2, 9.8, and 34.1 μg/kg were administered to animals QAD for 10 days (five total doses). CCW702 administration was generally well tolerated at these dose levels with no changes in animal body weight, food consumption, or body temperature and the no-observed-adverse-effect level (NOAEL) determined to be the highest dose in the study of 34.1 μg/kg. CCW702 induced transient and dose-dependent up-regulation of cytokines and redistribution of T cell populations, consistent with the mechanism of action. Of the 17 cytokines measured, increases in IL-10, IL-2, IL-1Ra, IL-6, IL-8, monocyte chemoattractant protein 1 (MCP-1), macrophage inflammatory protein-β (MIP-β), and TNF-α occurred earliest and peaked between approximately 2 and 8 hours after the first dose (Fig. 6A and fig. S18, A to C). IL-1β, IL-17, and granulocyte-macrophage colony-stimulating factor (GM-CSF) were not detected in any animals. All measured cytokines decreased significantly by 24 hours after the first dose. Notably, cytokine levels after the fifth dose of CCW702 (on day 9) were significantly reduced in the higher-dose groups (9.8 and 34.1 μg/kg) compared with the first dose. This occurred despite similar exposure of CCW702 on day 1 and on day 9 (1.02 hours·μg/ml versus 0.705 hours·μg/ml for the 34.1 μg/kg group) (fig. S17). This was putatively due to tachyphylaxis after multiple doses in these groups. CD4 and CD8 T cell counts corroborated this phenomenon with significant decreases in peripheral blood by 4 hours after the first dose, which trended higher by the fifth dose (Fig. 6B).

DISCUSSION

Bispecific antibodies have the potential to be transformative therapies for patients with cancer, but their development has been challenged by difficulties in engineering, poor biophysical properties, immunogenicity, and short half-life (*7*, *9*). Here, we leveraged the semisynthetic format of CCW702 to address these challenges. To optimize function, site-specific unnatural amino acid conjugation was used to assess the optimal valency and geometry of CD3 and PSMA engagement created through variation of the conjugation point of DUPA to the anti-CD3 Fab (*10*). This contrasts with fully recombinant bispecific technologies, such as bis-scFv or knob-in-hole approaches, which are generally fixed in the orientation of the CD3-binding domain relative to their antigen-targeting domain (*39*). Conjugating DUPA to the HC of the huL5H2_DI Fab (1× HC) produced a more potent molecule compared to conjugation to both the HC and the LC (2× LC/HC). This negative contribution of the 1× LC orientation to the 2× LC/HC construct suggests that 1× LC forms a suboptimal immunological synapse, which is less productive than 1× HC. The influence of binding orientation to the formation of productive versus nonproductive immunological synapses is supported by previous work from us and others and underscores the importance of optimization (*39*, *40*).

Another advantage of the semisynthetic format is that it uses the most stable portion of the antibody, the C_H1 domain [domain 1 of the constant portion of the immunoglobulin (Ig) HC], in a native chain-pairing orientation that lacks added protein-based linkers.

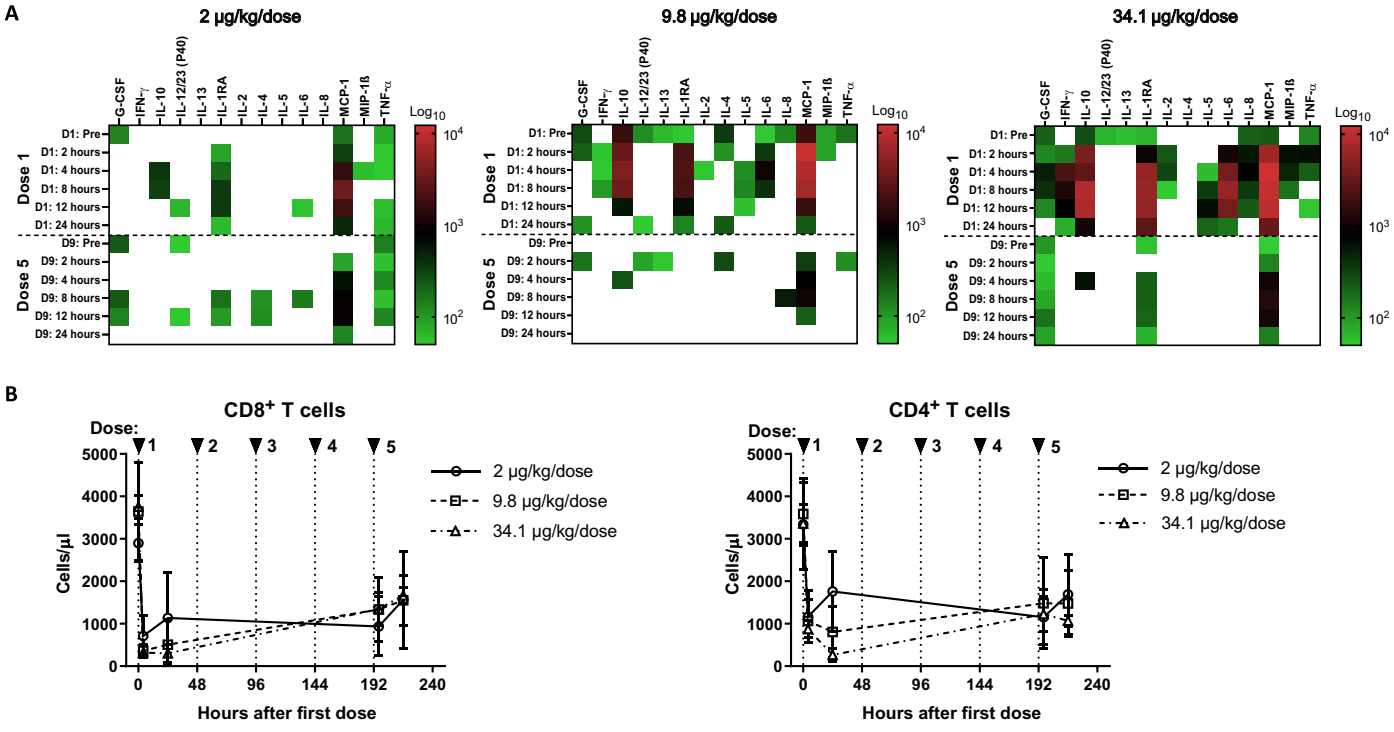

Fig. 6. Pharmacodynamics of CCW702 administered subcutaneously to male cynomolgus monkeys. (**A**) Heatmaps of cytokines measured from peripheral blood of animals administrated CCW702 at 2, 9.8, and 34.1 µg/kg, every other day for 10 days (a total of five total doses). Time points of collection at the left represent hours after the first dose (day 1) and the fifth dose (day 9), separated by a horizontal dashed line. Log_2 color scale: red, 10^4 pg/ml; black 10^3 pg/ml; and green, 10^2 pg/ml. No color (white) indicates that detection was below limit of quantification. (**B**) Enumeration of CD8 (left) and CD4 (right) T cells by flow cytometry from animals administrated with CCW702 at 2, 9.8, and 34.1 µg/kg, sampled after the first and last dose of CCW702. Black triangles with numbers and vertical dotted lines represent dose.

This format is less prone to aggregation, compared with bis-scFv–based formats, which may form aggregates because of "domain exchange" (*10*, *28*, *39*). Furthermore, the lack of non-native protein linkers reduces the potential for introduction of T cell epitopes, which play an important role in the development of ADA responses to biologics. To further mitigate the potential for immunogenicity, we used the EpiMatrix (EpiVax Inc.) to eliminate identified T cell epitopes through the incorporation of four mutations in the HC (*27*). While potential for the induction of an immune response to the small molecule P-TriA-DUPA cannot be taken into account using this approach, the resulting overall EpiMatrix score of the huL5H2_DI Fab was comparable to palivizumab and trastuzumab, which have low incidences of immunogenic responses in human (fig. S3). Assessment in patients will be necessary to determine the incidence of ADA responses and whether these responses are neutralizing.

CCW702's optimized, stable bispecific format resulted in picomolar-level PSMA-positive cell lysis in vitro with no activity against PSMA-negative cells even at concentrations of 10^4-fold above the EC_{50}. Notably, bell-shaped curves indicating autoinhibition or prozone effects were not observed in any of the in vitro activity assays even at these high concentrations. This may indicate that CCW702 achieved optimal three-body binding equilibria between the target cell, CCW702, and T cell (*41*). In vitro, the most sensitive assay of biologic activity was target cell cytotoxicity, compared with cytokine release or up-regulation of T cell activation markers, consistent with reports for other bispecific antibodies (*30*). Thus, the capacity to induce T cell–mediated tumor cell lysis occurred at lower concentrations of CCW702 than concentrations that elicit a cytokine production (*42*). Because cytokine release syndrome is a frequent adverse event associated with T cell agonistic antibodies, a lower threshold for cytotoxicity may be important in the ability to establish a therapeutic index in humans. Accordingly, using the most sensitive assay of activity to develop a minimal anticipated biological effect level (MABEL) is a recommended approach to determining the maximum recommended starting dose in clinical trials (*43*).

CCW702 also demonstrated antigen density–dependent target cell lysis, which is expected to facilitate the discrimination of PSMA on prostate cancer cells from low levels of PSMA expressed on healthy/normal tissues, including salivary glands, a subset of proximal renal tubules, and the duodenal brush border (*15*, *44*). Notably, in the clinical testing of DUPA-based radiotherapeutics, renal toxicity was reported as generally low (*45*) with dose-dependent xerostomia noted (*46*). This further supports the potential to selectively target PSMA-positive tumor over healthy tissue.

In in vivo studies, CCW702 demonstrated complete elimination of tumors in a C4-2 xenograft model over a wide range of dose concentrations and regimens. Human T cells were adoptively transferred into immunodeficient mice because of the lack of cross-reactivity of CCW702 with mouse T cells. Three doses of CCW702 administered subcutaneously weekly at 3.5 mg/kg cleared tumor, similar to the comparator pasotuxizumab, which was dosed daily 3.75 mg/kg subcutaneously as previously reported (*12*). This dosing regimen for CCW702 amounted to just three doses. On the basis of the short half-life of CCW702 in mice, it is not expected that this dosing regimen

resulted in continuous plasma exposure in the predicted therapeutic range. Thus, continuous on-target exposure of CCW702 may not be required for antitumor efficacy in the xenograft mouse model. Further studies to assess tumor-infiltrating T cells in patients treated with CCW702 will provide insights into the dose-efficacy relationship. In addition, in vivo testing of CCW702 in the patient-derived xenograft (PDX) model PCSD1 showed that CCW702 was able to eliminate tumors in the bone, a typically therapy-resistant site in the PDX model and in patients.

In cynomolgus monkey, CCW702 demonstrated near complete subcutaneous bioavailability with a C_{max} nearly 20-fold lower compared with intravenous dosing, and an 11.4-hour half-life. The lowered C_{max} via the subcutaneous route of administration is expected to mitigate the potential for cytokine release syndrome—a C_{max}-driven toxicity associated with T cell agonistic agents (*43*). The half-life and relatively "flat" pharmacokinetics profile of subcutaneous dosing in nonhuman primate, in addition to the Q7D mouse model efficacy data, support the potential to test a weekly dosing regimen in the clinic. This is expected to be a significant advantage from a patient convenience and compliance perspective compared with continuous infusion, which is required for other bispecific antibodies that have very short half-lives, such as blinatumomab (*47*). Notably, although CCW702 has a similar size compared with blinatumomab (approximately 50 kDa), it has a significantly longer projected half-life compared with blinatumomab (1.25 ± 0.63 hours) (*48*)). This small size is expected to facilitate tumor penetration compared with large-format bispecifics that use an Fc domain for extended half-life (*49*).

CCW702 induced dose-dependent up-regulation of cytokines and extravasation of T cells in peripheral blood of cynomolgus monkeys, consistent with the reactivity of CCW702 with cyno PSMA and CD3. Notably, multiple doses of CCW702 induced a tachyphylactic effect on T cells with the fifth dose producing a weaker amplitude of cytokine response than the first dose, despite comparable exposure of CCW702 (*50*). This nonmonotonic dose-toxicity curve has been well described for bispecific antibodies and may support use of a step dose, or priming dosing, as is used for several bispecifics in clinical testing, including the U.S. Food and Drug Administration–approved CD19-bispecific antibody blinatumomab (*47*). In summary, the studies reported here provide the efficacy, pharmacology, and differentiated design attributes that support the testing of CCW702 in patients. CCW702 is currently in phase 1 testing for patients with mCRPC (NCT04077021).

MATERIALS AND METHODS

Cell lines, PDX, and human T cells

C4-2 cells were purchased from Urocor Inc., and DU145, LNCaP, VCaP, and 22Rv-1 cells were purchased from the American Type Culture Collection and cultured as per the supplier's instructions. Human PBMCs were obtained via Ficoll-Pacque from normal donor whole blood from The Scripps Research Institute's Normal Blood Donor Service at Scripps General Clinical Research Center, under The Scripps Research Institute's Institutional Review Board (IRB) approval. For assays that used PBMCs, purified PBMCs were incubated in flasks in RPMI 1640 medium with 10% (v/v) fetal bovine serum (FBS) for 1 hour to remove adherent cells. For activated T cells, T cells were activated using CD3/CD28 Dynabeads (Thermo Fisher Scientific) and subsequently expanded in Aim-V media supplemented with 5% (v/v) heat-inactivated human serum (Valley Biomedical) and 300 IU/ml IL-2 (R&D Systems). For the in vivo PDX model, the study was carried out in strict accordance with the recommendations in the guide for the University of California San Diego (UCSD) IRB protocol number 090401. Approval was received from the UCSD IRB to collect surgical specimens from a patient for research purposes. For all experiments involving human participants, informed consent was obtained from all participants. A surgical prostate cancer bone metastasis deidentified specimen was harvested from a patient who progressed to castrate-resistant bone metastatic prostate cancer, which was named PCSD1. Intrafemoral injection of PCSD1 was performed to establish a PDX model representing a preclinical model of bone metastatic prostate cancer as previously shown (*35–37*). All animal protocols were performed under a UCSD animal welfare Institutional Animal Care and Use Committee–approved protocol.

Production of anti-CD3 Fab–DUPA conjugates

Production and conjugation DUPA-CD3 conjugates using oxime ligation was carried out as previously described in (*10*) and (*51*) and as depicted in fig. S2. Briefly, anti-CD3 Fab sequences inserted 3′ of a STII leader peptide in a vector that harbors the suppressor transfer RNA (tRNA) E9RS aminoacyl-tRNA synthase. To enable site-specific unnatural amino acid incorporation for DUPA conjugation, the following residues were mutated to the TAG amber nonsense codon, where indicated (UCHT1 at HC residue K138 and/or LC residue S202; huL5H2-based conjugates at HC residue K141 or LC residue S205). Production of Fabs was carried out in *Escherichia coli*, with media containing the unnatural amino acid *p*-acetylphenylalanine. Fabs were purified using CaptureSelect IgG-CH1 affinity matrix (Thermo Fisher Scientific) and eluted using low-pH buffer. Conjugation was carried out with similar conditions as previously described (*10*), using 30 to 40 molar excess of DUPA-linker in 50 mM sodium acetate buffer (pH 4.5). Conjugations were carried out for 24 to 48 hours. Subsequent buffer exchange and polishing by strong cation exchanger resin SP Sepharose Fast Flow (GE Healthcare Life Sciences) were performed to remove free, nonconjugated DUPA-linker.

Flow cytometry–based binding

Binding activity of humanized Fabs specific for human and cynomolgus CD3 were evaluated by flow cytometry. Briefly, cells were incubated with humanized Fabs at 4°C for 30 min and washed twice with staining buffer (1% bovine serum albumin in PBS). Bound antibodies were revealed with R-phycoerythrin–conjugated anti-human κ secondary antibodies (Southern Biotech). After several washes, samples were acquired on a BD LSR II or BD Accuri C6 and analyzed using FlowJo 7.6.2 software. In each study, observed the mean fluorescence intensity of cells incubated with secondary antibody alone was used to subtract for background and nonspecific staining.

In vitro coculture (cytotoxicity) assays

Target cells were dissociated with 0.05% trypsin/EDTA solution (HyClone) and washed with RPMI 1640 with 10% (v/v) FBS. Target cells were mixed with PBMCs at a 1:10 ratio in 100 μl of RPMI 1640 with 10% (v/v) FBS and incubated with indicated concentrations of conjugates, 24 hours, 37°C. Cytotoxicity was measured by quantification of lactate dehydrogenase (LDH) in supernatant using the CytoTox 96 nonradioactive cytotoxicity assay kit (Promega). Maximum target cell lysis was afforded via additional lysis solution and instructions per the manufacturer. Spontaneous killing was measured in wells with effector and target cells treated with vehicle (10 μl of PBS).

Absorbance at 490 nm was recorded using a SpectraMax 250 plate reader (Molecular Devices Corp.). Where indicated, supernatant was removed to quantify cytokines [(Human T_h1/T_h2 Cytokine Bead Array Kit II (CBA; BD)]. Percent cytotoxicity was calculated by the following equation: % Cytotoxicity = (absorbance experimental – absorbance spontaneous average)/(absorbance maximum killing average – absorbance spontaneous average).

C4-2 xenograft model

NSG mice (the Jackson Laboratories) were injected subcutaneously with C4-2 cells (2.5×10^6 cells per mouse) resuspended in 1:1 PBS:Matrigel. Tumors were engrafted for 7 days. On day 8, when tumors reached ~200 mm^3, mice were injected intraperitoneally with expanded T cells (20×10^6 per mouse). On day 9, CCW702 at the indicated routes of administration (intravenously or subcutaneously), regimens [every other day (QAD), every four days (Q4D), or every seven days (Q7D)], and at the indicated doses was administered for 20 days (QAD, 10 doses; Q4D, 5 doses; and Q7D, 3 doses). Groups with tumor only (no T cells and no CCW702) and only tumor with T cells (no CCW702) were used as controls. Pasotuxizumab dosed every day (QD) for 28 days at 3.75 mg/kg, subcutaneously, was used as benchmark control. Tumor volume was determined by caliper measurements and tumor volumes calculated using the following formula (long axis/2 × short $axis^2$). Mice were bled 24 hours after the first dose, and cytokines were analyzed on serum by a multiplexed sandwich immunoassay for three cytokines (IL-2, IFN-γ, and TNF-α) using a MESO QuickPlex SQ 120 detection system. On day 18, after tumor cell injection, mice were bled for T cell (CD3, CD4, and CD8) enumeration by flow cytometry using CountBright Absolute Counting Beads (Thermo Fisher Scientific).

PCSD1 green fluorescent protein–luciferase PDX model

Model was conducted as previously described ((*37*) and (*36*)). Briefly, green fluorescent protein–luciferase PCSD1 cells were injected intrafemorally (2.5×10^4 cells in 15 μl per mouse) into the right femur of 6-week-old male NSG mice (the Jackson Laboratories). Mice were monitored weekly for health, body weight, and appearance of palpable tumor. Tumor engraftment was confirmed using in vivo bioluminescence measured in a Xenogen IVIS 200 system (IVIS 200; PerkinElmer Inc.) within the Moores Cancer Center Vivarium immunodeficient mouse area. IVIS imaging was performed once per week and just before euthanizing mice at the termination of the experiment. Once the tumor reached a minimum of 200 to 400 mm^3 by caliper measurement, at approximately 6 weeks after implantation, mice were randomized into treatment groups. Activated T cells (20×10^6/100 μl in PBS per mouse) were injected intraperitoneally on day 30. Starting the next day (day 31), mice received daily intravenous injections of 100 μl of PBS or CCW702 for a total of 10 days. Mice were weighed, health status recorded, and tumors measured using calipers twice a week. Tumor volume was calculated using the formula: Tumor volume (mm^3) = [length (mm) × width (mm^2) × 0.5]. Caliper measurements in the intrafemoral model include the upper leg because of the location of the tumor. Treatment was reinitiated for additional 10 doses upon tumor relapse. Tumor volume was also assessed using an in vivo bioluminescence imaging system (IVIS 200; PerkinElmer Inc.) once per week. When tumors reached the maximal allowable size of 2.0 cm in length by caliper measurement, the mice were euthanized according to UCSD Animal Care Program standards.

Pharmacokinetic and pharmacodynamic 10-day study in cynomolgus monkeys dosed QOD with CCW702 (non-Good Laboratory Practice)

Nine naïve male cynomolgus monkeys (*Macaca fascicularis*, Chinese origin), age 2 to 4 years, weighing 2.5 to 3.2 kg were used for the study. Animals were randomly assigned to three dosing groups (three animals per group). The study and all analyses were carried out at Charles River Laboratories. There were no CCW702-related clinical signs, changes in body weight, food consumption (qualitative), body temperature, or macroscopic findings at terminal necropsy, and all animals survived until necropsy. Dose administration of >2 μg/kg per dose was associated with clinical pathology changes and microscopic findings that were not determined to be adverse. CCW702-related microscopic findings at terminal necropsy present in the >2 μg/kg per dose included perivascular mononuclear to mixed cell infiltrates in the adrenal gland, epididymis, kidney, liver, prostate, seminal vesicle, and subcutaneous administration sites, and increased cellularity of the bone marrow. The minimal to mild perivascular mononuclear to mixed cellular infiltrates in the adrenal medulla were of unknown biological significance. The NOAEL was determined to be 34.1 μg/kg under the study conditions. Cytokines collected in K2EDTA tubes and analyzed by a multiplexed immunoassay for 17 cytokines/chemokines [IL-1β, IL-1ra, IL-2, IL-4, IL-5, IL-6, IL-8, IL-10, IL-12/23 (p40), IL-13, IL-17, G-CSF, GM-CSF, IFN-γ, TNF-α, MCP-1, and MIP-1β)] using a Luminex detection system and a validated analytical method. Flow cytometry samples were collected in BD TruCount tubes in combination with CD45 labeling for real-time quantification of lymphocyte absolute counts. Samples were analyzed utilizing the FACSCanto II Flow Cytometer and DIVA 6.1.3 software. CD4 cells were gated as $CD45^+/CD4^+/CD8^-$ and CD8 cells were gated as $CD45^+/CD8^-/CD4^+$. The following equations were used for this data analysis: Total cell count = {[number of events in the lymphocytes region (R1)] / [number of events in the TruCount beads region (R2)]} × {[number of beads per test (as per insert)] / [test volume (50 μl)]}; absolute count = % gated × total cell count / 100.

SUPPLEMENTARY MATERIALS

Supplementary material for this article is available at http://advances.sciencemag.org/cgi/content/full/7/33/eabi8193/DC1

REFERENCES AND NOTES

1. R. L. Siegel, K. D. Miller, A. Jemal, Cancer statistics, 2019. *CA Cancer J. Clin.* **69**, 7–34 (2019).
2. J. A. Brockman, S. Alanee, A. J. Vickers, P. T. Scardino, D. P. Wood, A. S. Kibel, D. W. Lin, F. J. Bianco Jr., D. M. Rabah, E. A. Klein, J. P. Ciezki, T. Gao, M. W. Kattan, A. J. Stephenson, Nomogram predicting prostate cancer-specific mortality for men with biochemical recurrence after radical prostatectomy. *Eur. Urol.* **67**, 1160–1167 (2015).
3. G. Facchini, O. Caffo, C. Ortega, C. D'Aniello, M. Di Napoli, S. C. Cecere, C. Della Pepa, A. Crispo, F. Maines, F. Ruatta, G. Iovane, S. Pisconti, M. Montella, M. Berretta, S. Pignata, C. Cavaliere, Very early PSA response to abiraterone in mCRPC patients: A novel prognostic factor predicting overall survival. *Front. Pharmacol.* **7**, 123 (2016).
4. R. de Wit, J. de Bono, C. N. Sternberg, K. Fizazi, B. Tombal, C. Wulfing, G. Kramer, J. C. Eymard, A. Bamias, J. Carles, R. Iacovelli, B. Melichar, A. Sverrisdottir, C. Theodore, S. Feyerabend, C. Helissey, A. Ozatilgan, C. Geffriaud-Ricouard, D. Castellano; CARD Investigators, Cabazitaxel versus abiraterone or enzalutamide in metastatic prostate cancer. *N. Engl. J. Med.* **381**, 2506–2518 (2019).
5. B. T. Rekoske, D. G. McNeel, Immunotherapy for prostate cancer: False promises or true hope? *Cancer* **122**, 3598–3607 (2016).
6. K. G. Anderson, I. M. Stromnes, P. D. Greenberg, Obstacles posed by the tumor microenvironment to t cell activity: A case for synergistic therapies. *Cancer Cell* **31**, 311–325 (2017).
7. S. R. Frankel, P. A. Baeuerle, Targeting T cells to tumor cells using bispecific antibodies. *Curr. Opin. Chem. Biol.* **17**, 385–392 (2013).

8. T. Ishiguro, Y. Sano, S. I. Komatsu, M. Kamata-Sakurai, A. Kaneko, Y. Kinoshita, H. Shiraiwa, Y. Azuma, T. Tsunenari, Y. Kayukawa, Y. Sonobe, N. Ono, K. Sakata, T. Fujii, Y. Miyazaki, M. Noguchi, M. Endo, A. Harada, W. Frings, E. Fujii, E. Nanba, A. Narita, A. Sakamoto, T. Wakabayashi, H. Konishi, H. Segawa, T. Igawa, T. Tsushima, H. Mutoh, Y. Nishito, M. Takahashi, L. Stewart, E. ElGabry, Y. Kawabe, M. Ishigai, S. Chiba, M. Aoki, K. Hattori, J. Nezu, An anti-glypican 3/CD3 bispecific T cell-redirecting antibody for treatment of solid tumors. *Sci. Transl. Med.* **9**, eaal4291 (2017).
9. N. Hollander, Bispecific antibodies for cancer therapy. *Immunotherapy* **1**, 211–222 (2009).
10. C. H. Kim, J. Y. Axup, B. R. Lawson, H. Yun, V. Tardif, S. H. Choi, Q. Zhou, A. Dubrovska, S. L. Biroc, R. Marsden, J. Pinstaff, V. V. Smider, P. G. Schultz, Bispecific small molecule-antibody conjugate targeting prostate cancer. *Proc. Natl. Acad. Sci. U.S.A.* **110**, 17796–17801 (2013).
11. G. Hernandez-Hoyos, T. Sewell, R. Bader, J. Bannink, R. A. Chenault, M. Daugherty, M. Dasovich, H. Fang, R. Gottschalk, J. Kumer, R. E. Miller, P. Ravikumar, J. Wiens, P. A. Algate, D. Bienvenue, C. J. McMahan, S. K. Natarajan, J. A. Gross, J. W. Blankenship, MOR209/ES414, a novel bispecific antibody targeting PSMA for the treatment of metastatic castration-resistant prostate cancer. *Mol. Cancer Ther.* **15**, 2155–2165 (2016).
12. M. Friedrich, T. Raum, R. Lutterbuese, M. Voelkel, P. Deegen, D. Rau, R. Kischel, P. Hoffmann, C. Brandl, J. Schuhmacher, P. Mueller, R. Finnern, M. Fuergut, D. Zopf, J. W. Slootstra, P. A. Baeuerle, B. Rattel, P. Kufer, Regression of human prostate cancer xenografts in mice by AMG 212/BAY2010112, a novel PSMA/CD3-Bispecific BiTE antibody cross-reactive with non-human primate antigens. *Mol. Cancer Ther.* **11**, 2664–2673 (2012).
13. J. T. Patterson, J. Isaacson, L. Kerwin, G. Atassi, R. Duggal, D. Bresson, T. Zhu, H. Zhou, Y. Fu, G. F. Kaufmann, PSMA-targeted bispecific Fab conjugates that engage T cells. *Bioorg. Med. Chem. Lett.* **27**, 5490–5495 (2017).
14. P. Buhler, P. Wolf, D. Gierschner, I. Schaber, A. Katzenwadel, W. Schultze-Seemann, U. Wetterauer, M. Tacke, M. Swamy, W. W. Schamel, U. Elsässer-Beile, A bispecific diabody directed against prostate-specific membrane antigen and CD3 induces T-cell mediated lysis of prostate cancer cells. *Cancer Immunol. Immunother.* **57**, 43–52 (2008).
15. D. A. Silver, I. Pellicer, W. R. Fair, W. D. Heston, C. Cordon-Cardo, Prostate-specific membrane antigen expression in normal and malignant human tissues. *Clin. Cancer Res.* **3**, 81–85 (1997).
16. S. D. Sweat, A. Pacelli, G. P. Murphy, D. G. Bostwick, Prostate-specific membrane antigen expression is greatest in prostate adenocarcinoma and lymph node metastases. *Urology* **52**, 637–640 (1998).
17. B. Meller, F. Bremmer, C. O. Sahlmann, S. Hijazi, C. Bouter, L. Trojan, J. Meller, P. Thelen, Alterations in androgen deprivation enhanced prostate-specific membrane antigen (PSMA) expression in prostate cancer cells as a target for diagnostics and therapy. *EJNMMI Res.* **5**, 66 (2015).
18. G. L. Wright Jr., B. M. Grob, C. Haley, K. Grossman, K. Newhall, D. Petrylak, J. Troyer, A. Konchuba, P. F. Schellhammer, R. Moriarty, Upregulation of prostate-specific membrane antigen after androgen-deprivation therapy. *Urology* **48**, 326–334 (1996).
19. S. R. Denmeade, A. M. Mhaka, D. M. Rosen, W. N. Brennen, S. Dalrymple, I. Dach, C. Olesen, B. Gurel, A. M. Demarzo, G. Wilding, M. A. Carducci, C. A. Dionne, J. V. Moller, P. Nissen, S. B. Christensen, J. T. Isaacs, Engineering a prostate-specific membrane antigen-activated tumor endothelial cell prodrug for cancer therapy. *Sci. Transl. Med.* **4**, 140ra186 (2012).
20. B. T. Ristau, D. S. O'Keefe, D. J. Bacich, The prostate-specific membrane antigen: Lessons and current clinical implications from 20 years of research. *Urol. Oncol.* **32**, 272–279 (2014).
21. S. A. Kularatne, K. Wang, H. K. Santhapuram, P. S. Low, Prostate-specific membrane antigen targeted imaging and therapy of prostate cancer using a PSMA inhibitor as a homing ligand. *Mol. Pharm.* **6**, 780–789 (2009).
22. A. P. Kiess, S. R. Banerjee, R. C. Mease, S. P. Rowe, A. Rao, C. A. Foss, Y. Chen, X. Yang, S. Y. Cho, S. Nimmagadda, M. G. Pomper, Prostate-specific membrane antigen as a target for cancer imaging and therapy. *Q. J. Nucl. Med. Mol. Imaging* **59**, 241–268 (2015).
23. S. Lutje, S. Heskamp, A. S. Cornelissen, T. D. Poeppel, S. A. van den Broek, S. Rosenbaum-Krumme, A. Bockisch, M. Gotthardt, M. Rijpkema, O. C. Boerman, PSMA ligands for radionuclide imaging and therapy of prostate cancer: Clinical status. *Theranostics* **5**, 1388–1401 (2015).
24. A. X. Zhang, R. P. Murelli, C. Barinka, J. Michel, A. Cocleaza, W. L. Jorgensen, J. Lubkowski, D. A. Spiegel, A remote arene-binding site on prostate specific membrane antigen revealed by antibody-recruiting small molecules. *J. Am. Chem. Soc.* **132**, 12711–12716 (2010).
25. Y. Chen, M. Pullambhatla, S. R. Banerjee, Y. Byun, M. Stathis, C. Rojas, B. S. Slusher, R. C. Mease, M. G. Pomper, Synthesis and biological evaluation of low molecular weight fluorescent imaging agents for the prostate-specific membrane antigen. *Bioconjug. Chem.* **23**, 2377–2385 (2012).
26. A. S. De Groot, W. Martin, Reducing risk, improving outcomes: Bioengineering less immunogenic protein therapeutics. *Clin. Immunol.* **131**, 189–201 (2009).
27. V. Jawa, L. P. Cousens, M. Awwad, E. Wakshull, H. Kropshofer, A. S. De Groot, T-cell dependent immunogenicity of protein therapeutics: Preclinical assessment and mitigation. *Clin. Immunol.* **149**, 534–555 (2013).
28. S. Choudhary, A. Parupudi (MedImmune, LLC, 2016), Formulations of bispecific antibodies, patent application PCT/US2015/047843.
29. M. L. Conrad, W. C. Davis, B. F. Koop, TCR and CD3 antibody cross-reactivity in 44 species. *Cytometry A* **71**, 925–933 (2007).
30. S. Dudal, H. Hinton, A. M. Giusti, M. Bacac, M. Muller, T. Fauti, S. Colombetti, T. Heckel, N. Giroud, C. Klein, P. Umana, L. Benincosa, J. Bachl, T. Singer, K. Bray-French, Application of a MABEL approach for a T cell-bispecific monoclonal antibody: CEA TCB. *J. Immunother.* **39**, 279–289 (2016).
31. U. Elsasser-Beile, P. Buhler, P. Wolf, Targeted therapies for prostate cancer against the prostate specific membrane antigen. *Curr. Drug Targets* **10**, 118–125 (2009).
32. R. D. Jachimowicz, G. Fracasso, P. J. Yazaki, B. E. Power, P. Borchmann, A. Engert, H. P. Hansen, K. S. Reiners, M. Marie, E. P. von Strandmann, A. Rothe, Induction of in vitro and in vivo NK cell cytotoxicity using high-avidity immunoligands targeting prostate-specific membrane antigen in prostate carcinoma. *Mol. Cancer Ther.* **10**, 1036–1045 (2011).
33. R. Lutterbuese, T. Raum, R. Kischel, P. Hoffmann, S. Mangold, B. Rattel, M. Friedrich, O. Thomas, G. Lorenczewski, D. Rau, E. Schaller, I. Herrmann, A. Wolf, T. Urbig, P. A. Baeuerle, P. Kufer, T cell-engaging BiTE antibodies specific for EGFR potently eliminate KRAS- and BRAF-mutated colorectal cancer cells. *Proc. Natl. Acad. Sci. U.S.A.* **107**, 12605–12610 (2010).
34. G. Molema, J. W. Tervaert, B. J. Kroesen, W. Helfrich, D. K. Meijer, L. F. de Leij, CD3 directed bispecific antibodies induce increased lymphocyte-endothelial cell interactions in vitro. *Br. J. Cancer* **82**, 472–479 (2000).
35. T. Hirata, S. C. Park, M. T. Muldong, C. N. Wu, T. Yamaguchi, A. Strasner, O. Raheem, H. Kumon, R. L. Sah, N. A. Cacalano, C. H. M. Jamieson, C. J. Kane, K. Masuda, A. A. Kulidjian, C. A. M. Jamieson, Specific bone region localization of osteolytic versus osteoblastic lesions in a patient-derived xenograft model of bone metastatic prostate cancer. *Asian J. Urol.* **3**, 229–239 (2016).
36. E. Godebu, M. Muldong, A. Strasner, C. N. Wu, S. C. Park, J. R. Woo, W. Ma, M. A. Liss, T. Hirata, O. Raheem, N. A. Cacalano, A. A. Kulidjian, C. A. Jamieson, PCSD1, a new patient-derived model of bone metastatic prostate cancer, is castrate-resistant in the bone-niche. *J. Transl. Med.* **12**, 275 (2014).
37. O. Raheem, A. A. Kulidjian, C. Wu, Y. B. Jeong, T. Yamaguchi, K. M. Smith, D. Goff, H. Leu, S. R. Morris, N. A. Cacalano, K. Masuda, C. H. Jamieson, C. J. Kane, C. A. Jamieson, A novel patient-derived intra-femoral xenograft model of bone metastatic prostate cancer that recapitulates mixed osteolytic and osteoblastic lesions. *J. Transl. Med.* **9**, 185 (2011).
38. J. A. Yanez, C. M. Remsberg, C. L. Sayre, M. L. Forrest, N. M. Davies, Flip-flop pharmacokinetics—Delivering a reversal of disposition: Challenges and opportunities during drug development. *Ther. Deliv.* **2**, 643–672 (2011).
39. P. A. Moore, W. Zhang, G. J. Rainey, S. Burke, H. Li, L. Huang, S. Gorlatov, M. C. Veri, S. Aggarwal, Y. Yang, K. Shah, L. Jin, S. Zhang, L. He, T. Zhang, V. Ciccarone, S. Koenig, E. Bonvini, S. Johnson, Application of dual affinity retargeting molecules to achieve optimal redirected T-cell killing of B-cell lymphoma. *Blood* **117**, 4542–4551 (2011).
40. D. T. Rodgers, M. Mazagova, E. N. Hampton, Y. Cao, N. S. Ramadoss, I. R. Hardy, A. Schulman, J. Du, F. Wang, O. Singer, J. Ma, V. Nunez, J. Shen, A. K. Woods, T. M. Wright, P. G. Schultz, C. H. Kim, T. S. Young, Switch-mediated activation and retargeting of CAR-T cells for B-cell malignancies. *Proc. Natl. Acad. Sci. U.S.A.* **113**, E459–E468 (2016).
41. E. F. Douglass Jr., C. J. Miller, G. Sparer, H. Shapiro, D. A. Spiegel, A comprehensive mathematical model for three-body binding equilibria. *J. Am. Chem. Soc.* **135**, 6092–6099 (2013).
42. Y. Itoh, R. N. Germain, Single cell analysis reveals regulated hierarchical T cell antigen receptor signaling thresholds and intraclonal heterogeneity for individual cytokine responses of CD4+ T cells. *J. Exp. Med.* **186**, 757–766 (1997).
43. H. Saber, P. Del Valle, T. K. Ricks, J. K. Leighton, An FDA oncology analysis of CD3 bispecific constructs and first-in-human dose selection. *Regul. Toxicol. Pharmacol.* **90**, 144–152 (2017).
44. S. Aggarwal, R. M. Ricklis, S. A. Williams, S. R. Denmeade, Comparative study of PSMA expression in the prostate of mouse, dog, monkey, and human. *Prostate* **66**, 903–910 (2006).
45. A. Yordanova, A. Becker, E. Eppard, S. Kurpig, C. Fisang, G. Feldmann, M. Essler, H. Ahmadzadehfar, The impact of repeated cycles of radioligand therapy using [177Lu] Lu-PSMA-617 on renal function in patients with hormone refractory metastatic prostate cancer. *Eur. J. Nucl. Med. Mol. Imaging* **44**, 1473–1479 (2017).
46. D. Taieb, J. M. Foletti, M. Bardies, P. Rocchi, R. J. Hicks, U. Haberkorn, PSMA-targeted radionuclide therapy and salivary gland toxicity: Why does it matter? *J. Nucl. Med.* **59**, 747–748 (2018).
47. A. Viardot, M. E. Goebeler, G. Hess, S. Neumann, M. Pfreundschuh, N. Adrian, F. Zettl, M. Libicher, C. Sayehli, J. Stieglmaier, A. Zhang, D. Nagorsen, R. C. Bargou, Phase 2 study of the bispecific T-cell engager (BiTE) antibody blinatumomab in relapsed/refractory diffuse large B-cell lymphoma. *Blood* **127**, 1410–1416 (2016).

48. C. A. Portell, C. M. Wenzell, A. S. Advani, Clinical and pharmacologic aspects of blinatumomab in the treatment of B-cell acute lymphoblastic leukemia. *Clin. Pharm.* **5**, 5–11 (2013).
49. P. Kufer, R. Lutterbuse, P. A. Baeuerle, A revival of bispecific antibodies. *Trends Biotechnol.* **22**, 238–244 (2004).
50. M. Kebenko, M. E. Goebeler, M. Wolf, A. Hasenburg, R. Seggewiss-Bernhardt, B. Ritter, B. Rautenberg, D. Atanackovic, A. Kratzer, J. B. Rottman, M. Friedrich, E. Vieser, S. Elm, I. Patzak, D. Wessiepe, S. Stienen, W. Fiedler, A multicenter phase 1 study of solitomab (MT110, AMG 110), a bispecific EpCAM/CD3 T-cell engager (BiTE®) antibody construct, in patients with refractory solid tumors. *Onco. Targets. Ther.* **7**, e1450710 (2018).
51. T. Javahishvili, A. Manibusan, S. Srinagesh, D. Lee, S. Ensari, M. Shimazu, P. G. Schultz, Role of tRNA orthogonality in an expanded genetic code. *ACS Chem. Biol.* **9**, 874–879 (2014).
52. V. Humblet, P. Misra, K. R. Bhushan, K. Nasr, Y. S. Ko, T. Tsukamoto, N. Pannier, J. V. Frangioni, W. Maison, Multivalent scaffolds for affinity maturation of small molecule cell surface binders and their application to prostate tumor targeting. *J. Med. Chem.* **52**, 544–550 (2009).
53. J. Foote, G. Winter, Antibody framework residues affecting the conformation of the hypervariable loops. *J. Mol. Biol.* **224**, 487–499 (1992).
54. C. A. Kettleborough, J. Saldanha, V. J. Heath, C. J. Morrison, M. M. Bendig, Humanization of a mouse monoclonal antibody by CDR-grafting: The importance of framework residues on loop conformation. *Protein Eng.* **4**, 773–783 (1991).

Acknowledgments: We thank K. Bonin for medical writing assistance. **Funding:** This study was supported by Wellcome Trust Translational award 103253/Z/13/Z. **Author contributions:** S.C.L., J.S.Y.M., and E.L. designed and performed in vitro and in vivo activity profiling. M.S.K. performed humanization. S.-H.C. and H.Y. synthesized DUPA-linker candidates, M.P. oversaw chemistry, E.N.H. expressed anti-CD3 proteins, and V.K. oversaw conjugation and production. S.C.L. and J.S.Y.M. carried out conjugations. C.J.K. and A.A.K. contributed to PDX experiment planning. M.T.M., C.N.W., W.M., and C.A.M.J. performed PDX models. A.K.W., V.N., and S.B.J. carried out in vivo xenograft models. S.C.L., S.B.J., J.W., and J.L. performed nonhuman primate toxicology and pharmacokinetics studies. P.G.S., C.H.K., and T.S.Y. led the design, planning, and execution of experiments. S.C.L. and T.S.Y. wrote the manuscript. **Competing interests:** S.C.L., J.S.Y.M., M.S.K., E.L., H.Y., P.G.S., C.H.K., and T.S.Y. are inventors on patent(s) and application(s) related to this work filed by The Scripps Research Institute. AbbVie has certain rights to the commercial development of CCW702. The authors declare that they have no other competing interests. **Data and materials availability:** Materials in this manuscript may be provided by Scripps Research (DUPA-CD3 conjugates) or University of California (PCSD1 cell line) subject to scientific review and material transfer agreement. Requests should be made to corresponding authors. All data needed to evaluate the conclusions in the paper are present in the paper and/or the Supplementary Materials.

Submitted 1 April 2021
Accepted 23 June 2021
Published 11 August 2021
10.1126/sciadv.abi8193

Citation: S. C. Lee, J. S. Y. Ma, M. S. Kim, E. Laborda, S.-H. Choi, E. N. Hampton, H. Yun, V. Nunez, M. T. Muldong, C. N. Wu, W. Ma, A. A. Kulidjian, C. J. Kane, V. Klyushnichenko, A. K. Woods, S. B. Joseph, M. Petrassi, J. Wisler, J. Li, C. A. M. Jamieson, P. G. Schultz, C. H. Kim, T. S. Young, A PSMA-targeted bispecific antibody for prostate cancer driven by a small-molecule targeting ligand. *Sci. Adv.* **7**, eabi8193 (2021).